Japanese Journal of Applied Physics
Vol. 45, No. 5B, 2006, pp. 4722–4726

Designing Beam Steering for Accurate Measurement of Intima-Media Thickness at Carotid Sinus

Takashi MASHIYAMA, Hideyuki HASEGAWA and Hiroshi KANAI*

Graduate School of Engineering, Tohoku University, Sendai 980-8579, Japan

(Received November 30, 2005; accepted February 22, 2006; published online May 25, 2006)

Recently, cardiovascular disease has become the second most common cause of death in Japan following malignant neoplasm formation. Therefore, it is necessary to diagnose atherosclerosis during its early stages because atherosclerosis is one of the main causes of cardiovascular diseases. The carotid sinus is a site that is easily affected by atherosclerosis [C. K. Zarins *et al.*: Circ. Res. **53** (1983) 502]; therefore, the diagnosis of this disease at this site is important [S. C. Nicholls *et al.*: Stroke **20** (1989) 175]. However, it is difficult to accurately diagnose atherosclerosis in the carotid sinus in the long-axis plane, which is parallel to the axis of the vessel, using conventional linear scanning because the carotid sinus is not flat along the axis of the vessel, and the ultrasonic beams used in linear scanning are perpendicular to the arterial wall in a limited region. Echoes from regions that are not perpendicular to the ultrasonic beams are very weak and the arterial wall in such regions is hardly recognized in a B-mode image. In this study, the position of the arterial wall was predetermined on the basis of the B-mode image obtained by conventional linear scanning, then ultrasonic beams were transmitted again so that all beams were almost perpendicular to the arterial wall. In basic experiments, a nonflat object made of silicone rubber was measured and it was shown that it is possible to image a nonflat object over the entire scanned area using the proposed beam steering method. Furthermore, in *in vivo* experiments, the intima–media complex was imaged over the entire scanned area at the carotid sinus. [DOI: 10.1143/JJAP.45.4722]

KEYWORDS: ultrasonic beam steering, intima–media thickness, carotid sinus, atherosclerosis

1. Introduction

Cardiovascular disease is now the second most common form of death in Japan following malignant neoplasm formation. The diagnosis of early-stage atherosclerosis has become increasingly important because atherosclerosis is one of the main causes of cardiovascular disease. The double line pattern of the arterial wall, which is shown in an ultrasound B-mode image, represents echoes from the lumen–intima and media–adventitia boundaries.[1)] The area between these two lines corresponds to the intima–media complex. The intima–media thickness (IMT) is a useful marker for the diagnosis of atherosclerosis.[1,2)] Cross sectional images of arteries are commonly obtained in the long-axis and short-axis planes, which are parallel and perpendicular to the axis of the artery, respectively. However, the intima–media complex is imaged in the short-axis plane in a limited region because ultrasonic beams are perpendicular to the wall in the limited region. Therefore, an alternative beam scanning method was developed so that the ultrasonic beams were always perpendicular to the arterial wall in the short-axis plane by assuming that the cross section of the artery lumen is a circle.[3)] Using this method, the IMT of the artery could be measured accurately in the short-axis plane, and this method was combined with the *phased tracking method* proposed by our group for measuring the regional strain and viscoelasticity of the arterial wall.[4–14)]

The carotid sinus is a site that is easily affected by atherosclerosis; therefore, the diagnosis of this disease at this site is important.[15,16)] However, it is difficult to diagnose atherosclerosis in this site in the long-axis plane accurately using conventional linear scanning because the carotid sinus is not flat along the axis of the vessel, and the ultrasonic beams used in linear scanning are perpendicular to the arterial wall in a limited region. Echoes from regions that are not perpendicular to the ultrasonic beams are very weak and the arterial wall in such regions is hardly recognized in a B-mode image. To improve the quality of B-mode images, multi angle compound imaging[17–19)] was developed. In this technique, images are recorded from multiple angles (typically 3 to 9), and these single-angle images are then combined to form the compound image. In most investigations on this technique so far, the individual single-angle images have been simply averaged to form the compound image.

In the method proposed in this study, the position of the arterial wall is predetermined on the basis of the B-mode image obtained by conventional linear scanning, then ultrasonic beams are transmitted again so that all beams are almost perpendicular to the arterial wall.

2. Principles

Figure 1 shows a schematic diagram of the beam steering. The ultrasonic beam scans M positions along the x-axis by conventional linear scanning. The depth of the arterial wall,

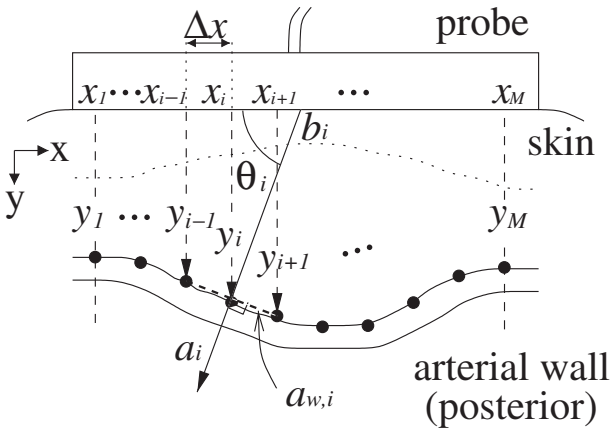

Fig. 1. Determination of optimum beam position and angle ($N = 1$).

*E-mail address: kanai@ecei.tohoku.ac.jp

y_i $(i = 1, 2, \ldots, M)$, at each beam position, x_i $(i = 1, 2, \ldots, M)$, is manually predetermined in the B-mode image obtained by conventional linear scanning. The interval between the neighboring ultrasonic beams is defined by $\Delta x = x_{i+1} - x_i$. With respect to each position, (x_i, y_i), of the i-th ultrasonic beam on the wall, a regional slope, $a_{w,i}$, of the arterial wall to the surface of the ultrasonic probe is estimated by the least-squares method using positions, $\{(x_i, y_i)\}$, of neighboring $\pm N$ ultrasonic beams on the arterial wall as follows:

$$a_{w,i} = \frac{(2N+1)\sum_{i=-N}^{N} x_i \cdot y_i - \left(\sum_{i=-N}^{N} x_i\right)\left(\sum_{i=-N}^{N} y_i\right)}{(2N+1)\sum_{i=-N}^{N} x_i^2 - \left(\sum_{i=-N}^{N} x_i\right)^2}. \quad (2.1)$$

From the estimated $a_{w,i}$, the slope, a_i, and the angle, θ_i, of the beam that is perpendicular to the arterial wall at (x_i, y_i) are determined as follows:

$$a_i = -\frac{1}{a_{w,i}}, \quad (2.2)$$

$$\theta_i = \tan^{-1} a_i \quad \text{(rad)}. \quad (2.3)$$

From the determined θ_i (rad) and the (x_i, y_i) of the arterial wall, the center, b_i, of the aperture that transmits an ultrasonic beam to (x_i, y_i) is determined as follows:

$$b_i = x_i - \frac{y_i}{\tan\theta_i} = x_i - \frac{y_i}{a_i} \quad \text{(mm)}. \quad (2.4)$$

By determining θ_i and b_i (mm) for all positions, $\{(x_i, y_i)\}$, on the wall, all beams are designed to be perpendicular to the arterial wall.

In this study, beam angles must be assigned by discrete values. Therefore, the discrete beam angle, θ_i', that is nearest to θ_i is selected from preassigned angles of K beams [Fig. 2(a)]. The b_i of the aperture is calculated again using θ_i'. The center of the aperture should be also assigned by a discrete value that depends on the element pitch of the ultrasonic probe. As shown in Fig. 2(b), the discrete transmit position, b_i', of the aperture, which is nearest to b_i, is selected, as well as θ_i'. In this way, the ultrasonic beam is transmitted to the position, (x_i', y_i'), on the wall as perpendicular as possible. Although the designed ultrasonic beam does not exactly pass through the (x_i, y_i) because of the discrete values of b_i' and θ_i', the difference, $|x_i' - x_i|$, is less than half the element pitch.

3. Basic Experiment

Figure 3 shows (a) the size and (b) cross section of a phantom made of silicone rubber. The shape of the phantom simulates the arterial wall at the carotid sinus and the phantom has a hollow. The width of the hollow is 15 mm, and the depth is 2.5 mm. Figure 4 shows the experimental system. The phantom was fixed in a water bath and it was measured using diagnostic equipment (Aloka SSD-6500) with a conventional linear-type ultrasonic probe at 10 MHz. The distance from the surface of the ultrasonic probe to the surface of the phantom was 13 mm. The focal distance was set to be 18 mm from the surface of the ultrasonic probe because the ultrasonic beam became wider and the measurement became more robust by setting the focal depth deeper than the surface of the phantom.[20,21] As schematically shown in Fig. 5, 105 ultrasonic beams with intervals, Δx, of 0.2 mm are transmitted in a frame, and the beam angle was changed by 2° frame by frame from $\theta_1' = 70°$ to $\theta_{21}' = 110°$. Therefore, the elapsed time for acquiring the RF data of 21 frames was 165 ms in the case of a frame rate of 127 Hz in this experiment. Ultrasonic RF echoes were acquired at a sampling frequency of 40 MHz.

Figure 6(a) shows a B-mode image of the object obtained

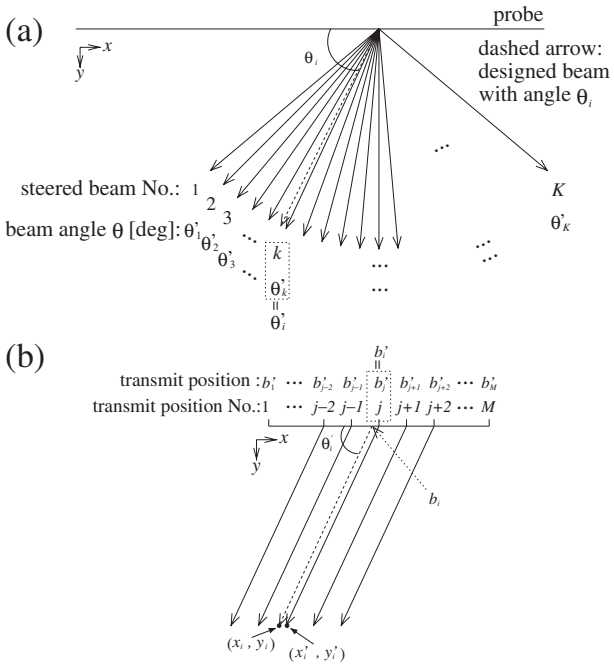

Fig. 2. (a) Determination of θ_i' (dashed line: calculated beam with θ_i). (b) Determination of b_i'.

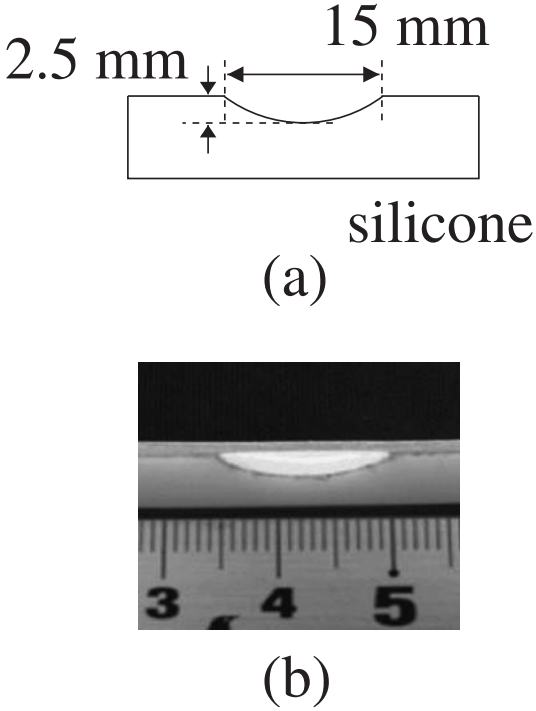

Fig. 3. (a) Size of phantom. (b) Cross sectional picture.

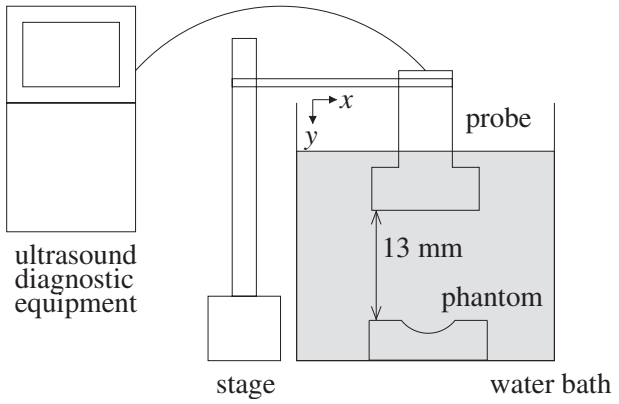

Fig. 4. Experimental system.

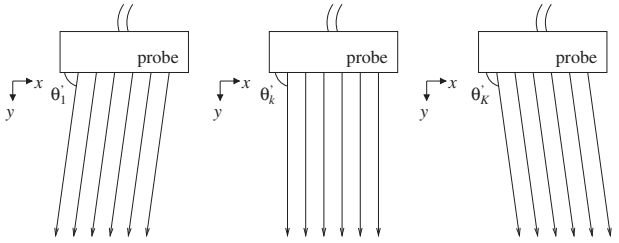

Fig. 5. Schematic diagram of beam scanning.

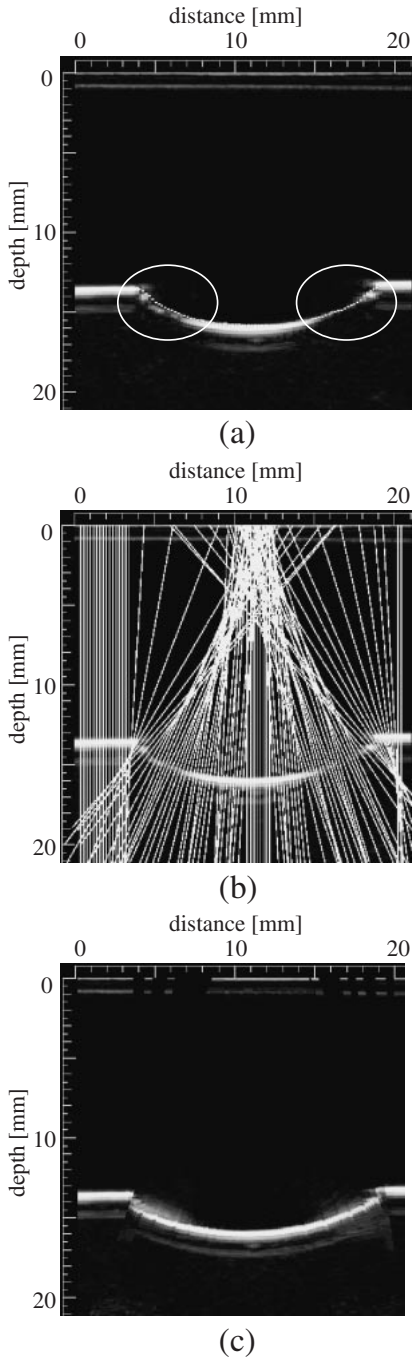

Fig. 6. (a) B-mode image obtained by conventional linear scanning (white dotted line: assigned silicone surface). (b) Calculated beams (white lines) superimposed on B-mode image. (c) B-mode image obtained by proposed method.

by conventional linear scanning using 105 ultrasonic beams ($\theta'_{11} = 90^\circ$). The surface of the phantom was manually assigned at 105 positions $\{(x_i, y_i)\}$ $(i = 1, 2, \ldots, 105)$ on the B-mode image [white dotted line in Fig. 6(a)]. On the basis of the principle in §2, the beam, with angle θ_i and transmit position b_i, that is perpendicular to the surface of the phantom was determined using $\{(x_i, y_i)\}$. The white lines in Fig. 6(b) show the calculated optimum beams. Then, the beam with θ'_i and b'_i was selected as shown in Fig. 2. Figure 6(c) shows a B-mode image constructed from the ultrasonic RF echoes obtained using the calculated beams with $\{(\theta'_i, b'_i)\}$.

As shown in the areas surrounded by circles in Fig. 6(a), the surface of the phantom could not be imaged clearly in the areas where the ultrasonic beams incline from a vertical direction by more than 20° as shown in the B-mode image obtained by conventional linear scanning. On the other hand, strong reflected echoes were obtained in such areas using the proposed method, and the phantom was imaged over the entire scanned area, as shown in Fig. 6(c).

4. *In Vivo* Experiment

A human common carotid sinus of a 25-year-old male was measured in the long-axis plane. To reduce the elapsed time for acquiring RF data, ultrasonic beams were transmitted every 5° from $\theta'_1 = 70^\circ$ to $\theta'_9 = 110^\circ$ and discrete steered angles, $\{\theta'_k\}$, were changed frame by frame. Ultrasonic RF data were acquired during nine frames (82 ms at a frame rate of 110 Hz) just before the time of the R-wave of the electrocardiogram. Figure 7(a) shows a B-mode image obtained by conventional linear scanning, composed of 105 ultrasonic beams with intervals, Δx, of 0.2 mm ($\theta'_5 = 90^\circ$). The white dotted line in Fig. 7(b) shows the assigned (x_i, y_i) of the posterior wall, and the white lines in Fig. 8(a) show the calculated optimum beams. Figure 8(b) shows a B-mode image constructed from the ultrasonic RF echoes obtained using the calculated beams with $\{(\theta'_i, b'_i)\}$. As shown by the area surrounded by a circle in Fig. 7(a), the intima–media complex could not be imaged clearly by conventional linear scanning in the area where the ultrasonic beams incline from the perpendicular direction relative to the wall by more than 2.5°. However, sufficient reflected echoes were obtained from such an area using the proposed method, and the intima–media complex was almost imaged over the entire scanned area as shown in Fig. 8(b).

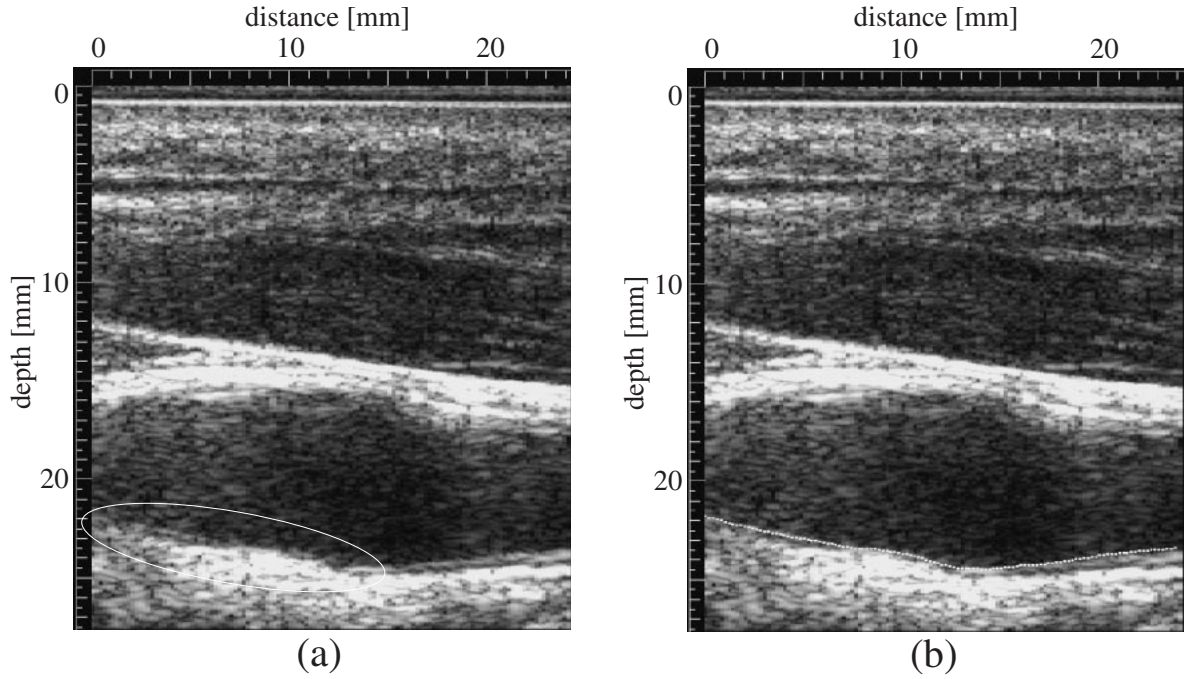

Fig. 7. (a) B-mode image obtained by conventional linear scanning. (b) Assigned posterior wall surface (white dashed line) superimposed on B-mode image of (a).

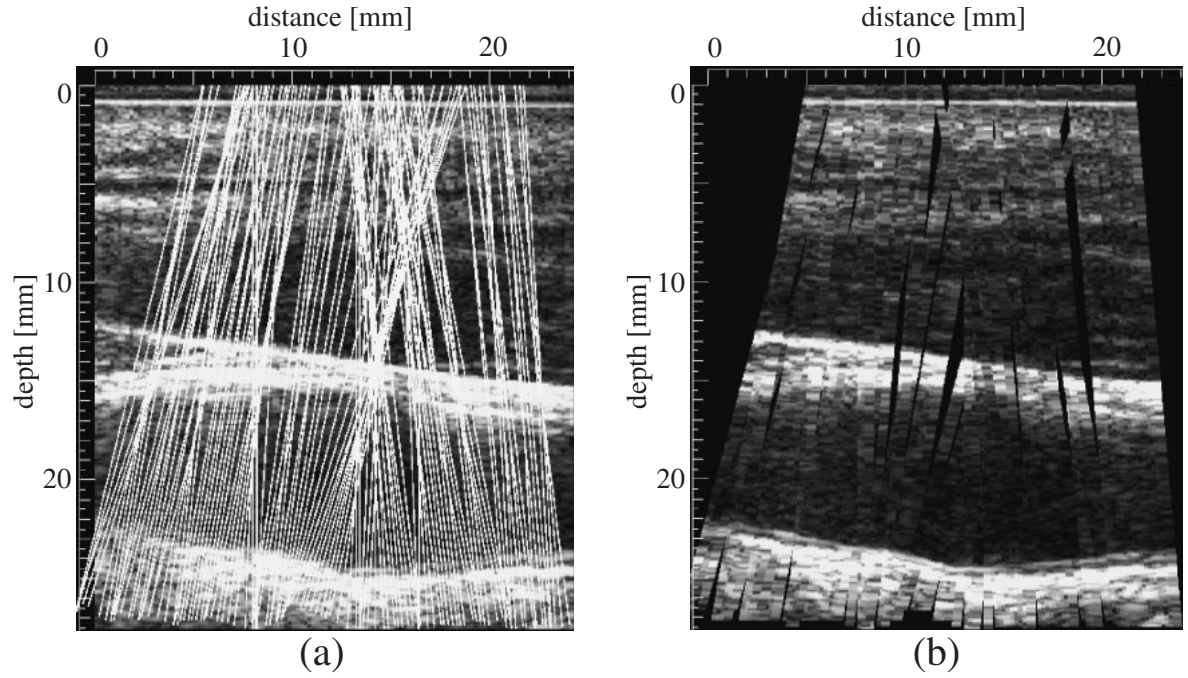

Fig. 8. (a) Calculated beams (white lines) superimposed on B-mode image of Fig. 7(a). (b) B-mode image obtained by proposed method.

5. Discussion

To realize the proposed method in a clinical situation, the following procedure is considered suitable. A B-mode image is obtained by conventional linear scanning, and positions on the arterial wall are detected automatically during a frame interval. Then, the ultrasonic beam that is perpendicular to the arterial wall is designed with respect to each detected position. In this case, frame rate does not decrease because one ultrasonic beam must be transmitted per assigned position on the wall. However, such a method for automatically detecting the position on the wall during a frame interval was not realized in this study. Therefore, RF data were acquired at various ultrasonic beam angles beforehand. In *in vivo* experiments, ultrasonic RF data were acquired during nine frames, which corresponds to 82 ms at a frame

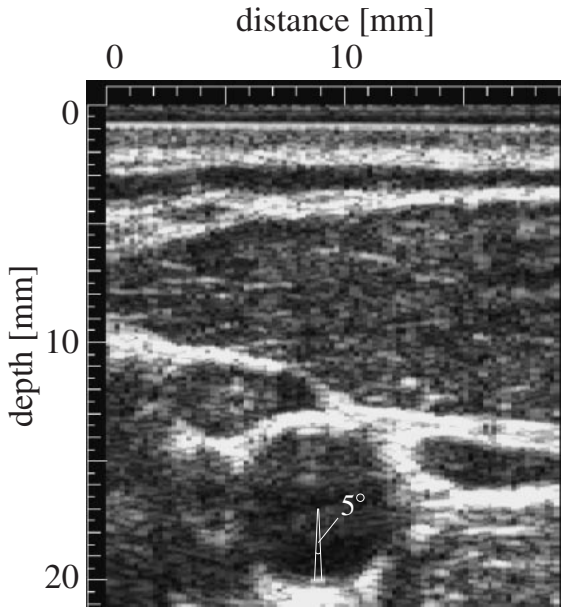

Fig. 9. B-mode image in short-axis plane obtained by conventional linear scanning.

rate of 110 Hz, and the increment step of the beam angle was increased to 5° in *in vivo* experiments to reduce the period for acquiring RF data to avoid the influence of movements of the arterial wall caused by the heartbeat. The increment step of 5° was determined as follows: Figure 9 shows a B-mode image of the carotid artery shown in Figs. 7 and 8 in the short-axis plane that is perpendicular to the axis of the artery. In Fig. 9, the intima–media complex of the posterior wall is imaged in the region where ultrasonic beams do not incline from the perpendicular insonification by more than 2.5°. Therefore, the increment step should be set to be at most 5°.

The period for acquiring RF data in this study is longer than a frame interval of 9 ms, and movements of the arterial wall caused by the heartbeat during this acquisition period may change the insonification angles of calculated beams from those expected by the proposed method. However, the intima–media complex was imaged as shown in Fig. 8(b) by setting the period for acquiring RF data to be just before the time of the R-wave of the electrocardiogram because the movement of the arterial wall is small in this phase of the heart cycle.

6. Conclusions

In this paper, a method of beam steering that makes ultrasonic beams perpendicular to the arterial wall at the carotid sinus in the long-axis plane was proposed. In basic experiments using a phantom made of silicone rubber, it was shown that it is possible to image a nonflat object over the entire scanned area using the proposed beam steering method. Furthermore, in *in vivo* experiments at a carotid sinus, it was shown that it is possible to image the intima–media complex over the entire scanned area using the proposed beam steering method.

1) A. D. M. van Swijndregt, S. H. K. The, E. J. Gussenhoven, C. T. Lancee, H. Rijsterborgh, E. de Groot, A. F. W. van der Steen, N. Bom and R. G. A. Ackerstaff: Ultrasound Med. Biol. **22** (1996) 1007.
2) A. D. M. van Swijndregt, E. E. de Lange, E. de Groot and R. G. A. Ackerstaff: Ultrasound Med. Biol. **25** (1999) 323.
3) N. Nakagawa, H. Hasegawa and H. Kanai: Jpn. J. Appl. Phys. **43** (2004) 3220.
4) H. Kanai, M. Sato, Y. Koiwa and N. Chubachi: IEEE Trans. Ultrason. Ferroelectr. Freq. Control **43** (1996) 791.
5) H. Kanai, Y. Koiwa and J. Zhang: IEEE Trans. Ultrason. Ferroelectr. Freq. Control **46** (1999) 1229.
6) H. Hasegawa, H. Kanai, N. Hoshimiya and Y. Koiwa: Jpn. J. Appl. Phys. **39** (2000) 3257.
7) H. Hasegawa, H. Kanai and Y. Koiwa: Jpn. J. Appl. Phys. **41** (2002) 3563.
8) H. Kanai, H. Hasegawa, M. Ichiki, F. Tezuka and Y. Koiwa: Circulation **107** (2003) 3018.
9) H. Hasegawa, H. Kanai, Y. Koiwa and J. P. Butler: Jpn. J. Appl. Phys. **42** (2003) 3255.
10) H. Hasegawa and H. Kanai: Jpn. J. Appl. Phys. **43** (2004) 3197.
11) J. Tang, H. Hasegawa and H. Kanai: Jpn. J. Appl. Phys. **44** (2005) 4588.
12) J. Inagaki, H. Hasegawa, H. Kanai, M. Ichiki and F. Tezuka: Jpn. J. Appl. Phys. **44** (2005) 4593.
13) H. Hasegawa and H. Kanai: Jpn. J. Appl. Phys. **44** (2005) 4609.
14) M. Sugimoto, H. Hasegawa and H. Kanai: Jpn. J. Appl. Phys. **44** (2005) 6297.
15) C. K. Zarins, D. P. Giddens, B. K. Bharadvaj, V. S. Sottiurai, R. F. Mabon and S. Glagov: Circ. Res. **53** (1983) 502.
16) S. C. Nicholls, D. J. Phillips, J. F. Primozich, R. L. Lawrence, T. R. Kohler, T. G. Rudd and D. E. Strandness: Stroke **20** (1989) 175.
17) A. Hernandez, O. Basset, P. Chirossel and G. Gimenez: Ultrasound Med. Biol. **22** (1996) 229.
18) S. K. Jespersen, J. E. Wilhjelm and H. Sillesen: Ultrasound Med. Biol. **26** (2000) 1357.
19) J. E. Wilhjelm, M. S. Jensen, S. K. Jespersen, B. Sahl and E. Falk: IEEE Trans. Med. Imaging **23** (2004) 181.
20) M. Watanabe and H. Kanai: Jpn. J. Appl. Phys. **40** (2001) 3918.
21) M. Watanabe, H. Hasegawa and H. Kanai: Jpn. J. Appl. Phys. **41** (2002) 3613.